# Two New Neutrophil Subsets Define a Discriminating Sepsis Signature

Aïda Meghraoui-Kheddar, Benjamin Chousterman, Noëlline Guillou, Sierra Barone, Samuel Granjeaud, Helene Vallet, Aurélien Corneau, Karim Guessous, Charles de Roquetaillade, Alexandre Boissonnas, et al.

HAL Id: hal-03419725

https://hal.sorbonne-universite.fr/hal-03419725

Submitted on 9 Feb 2022

# Two new neutrophil subsets define a discriminating sepsis signature

Aïda Meghraoui-Kheddar[1]*, Benjamin G. Chousterman [2,3], Noëlline Guillou[1], Sierra M. Barone[4], Samuel Granjeaud[5], Helene Vallet[1,6], Aurélien Corneau[7], Karim Guessous[2], Charles de Roquetaillade [2,3] Alexandre Boissonnas[1], Jonathan M. Irish[4, 8], Christophe Combadière[1]*

1   **Affiliations :**

2   [1] Sorbonne Université, Inserm, CNRS, Centre d'Immunologie et des Maladies Infectieuses, Cimi-Paris, F-75013, Paris, France.
3   [2] AP-HP, CHU Lariboisière, Department of Anesthesia and Critical Care, DMU Parabol, FHU Promice, Paris, France
4   [3] Université de Paris, Inserm U942 MASCOT, Paris, France
5   [4] Department of Cell and Developmental Biology, Vanderbilt University, Nashville, TN, USA
6   [5] CRCM, Inserm, U1068; Paoli-Calmettes Institute; Aix-Marseille University, UM 105; CNRS, UMR7258, Marseille, France.
7   [6] Acute geriatric unit, Saint Antoine Hospital, Assistance-Publique Hôpitaux de Paris, Paris, France.
8   [7] Sorbonne Université, UMS037, PASS, CyPS, Paris, France.
9   [8] Department of Pathology, Microbiology and Immunology, Vanderbilt University Medical Center, Nashville, TN, USA
10   * Corresponding author information :
11   Christophe Combadière, PhD,
12   Centre d'Immunologie et des Maladies Infectieuses (Cimi-Paris),
13   91 Boulevard de l'Hôpital, Faculté de Médecine Sorbonne université, site Pitié, 75013 Paris, France,
14   Tel: +33 140 779 897
15   e-mail: christophe.combadiere@upmc.fr
16   Aïda Meghraoui-Kheddar, PhD, PharmD,
17   Institut de Pharmacologie Moléculaire et Cellulaire, IPMC UMR7275,
18   660 route de Lucioles, Sophia Antipolis, 06560 Valbonne, France,
19   Tel: +33 4 93957781
20   e-mail: aida.meghraoui-kheddar@inserm.fr

21   **Authorship contributions:**

22   AMK, BGC, AB and CC designed the study. AMK and NG performed experimental work. BGC, KG, CdR
23   and HV provided clinical samples, pathological diagnosis and patient clinical data. AMK compiled patient
24   data. AMK and AC run samples in the mass cytometer. AMK, SMB, SG and JMI performed data analysis.
25   AMK, JMI and CC developed the figures, and wrote the manuscript. CC provided financial support. All
26   authors contributed in reviewing the manuscript.

27   **Running head:** Sepsis neutrophil signature for patients' diagnosis

28   **Subject Category:** 7.19 Neutrophils

29   **Text word count:** 4344

30   **At a Glance Commentary:**

31   There is an unmet need for specific and rapid diagnostic tests for sepsis, which would discriminate sepsis
32   patients from patients with aseptic inflammation. This work represents the first comprehensive evaluation of
33   whole blood circulating immune cells in septic patients using CyTOF high-dimensional technology coupled
34   with computational analysis. It allowed the identification of two novel sepsis-specific neutrophil subsets:
35   CD10-CD64+PD-L1+ and CD10-CD64+CD16low/-CD123+ immature neutrophils. This early sepsis immune
36   cell signature was validated computationally and biologically in an independent cohort and could be used for
37   sepsis diagnosis.

38 **Abstract**:

39 **Rationale:** Sepsis is the leading cause of death in adult intensive care units. At present, sepsis diagnosis relies

40 on non-specific clinical features. It could transform clinical care to have immune cell biomarkers that could

41 predict sepsis diagnosis and guide treatment. For decades, neutrophil phenotypes have been studied in sepsis,

42 but a diagnostic cell subset has yet to be identified.

43 **Objectives:** To identify an early specific immune signature of sepsis severity that does not overlap with other

44 inflammatory biomarkers, and that distinguishes patients with sepsis from those with non-infectious

45 inflammatory syndrome.

46 **Methods:** Mass cytometry combined with computational high-dimensional data analysis were used to measure

47 42 markers on whole blood immune cells from sepsis patients and controls, and automatically and

48 comprehensively characterize circulating immune cells, which enables identification of novel, disease-specific

49 cellular signatures.

50 **Measurements and Main Results:** Unsupervised analysis of high-dimensional mass cytometry data

51 characterized previously unappreciated heterogeneity within the $CD64^+$ immature neutrophils and revealed

52 two new subsets distinguished by CD123 and PD-L1 expression. These immature neutrophils exhibited

53 diminished activation and phagocytosis functions. The proportion of CD123-expressing neutrophils correlated

54 with clinical severity.

55 **Conclusions:** This study showed that these two new neutrophil subsets were specific to sepsis and detectable

56 by routine flow cytometry using seven markers. The demonstration here that a simple blood test distinguishes

57 sepsis from other inflammatory conditions represents a key biological milestone that can be immediately

58 translated into improvements in patient care.

59 **Abstract word count:** 232

60 **Key words:** Sepsis, neutrophils, diagnosis, PD-L1, CD123

## Introduction

Sepsis is the leading cause of death in the intensive care unit (ICU) (1-3). Diagnosis of patients relies on clinical data rather than a robust biomarker that distinguishes sepsis from sterile inflammation and predict its clinical outcome and prognosis can be evaluated by several scores including Simplified Acute Physiology Score II (SAPS II) and Sequential Organ Failure Assessment (SOFA) Score. SOFA and SAPS-II are indicators of severity, show poor performance regarding sepsis diagnostic and were consistently shown to be non-specific of sepsis (1, 4-7). It is estimated that the survival rate decreases by roughly 10% every hour that appropriate antimicrobial medication is delayed, emphasizing the urgent need for early diagnosis techniques (8, 9). A comprehensive systems immunology approach using mass cytometry is well-suited to characterize the diversity of disease-specific cellular states (10). Neutrophils are a primary immune cellular barrier against pathogens, but they may be a double-edged sword in sepsis having a role in both inflammation and immunosuppression (11-15). We hypothesized that phenotype of circulating neutrophils might provide crucial early insight into immune features that drive sepsis and distinguish this disease from non-infectious inflammatory syndrome.

For the systems immunology approach here, it was critical to track features that had been identified as important in sepsis biology, but which individually had not the resolving power to specifically distinguish sepsis. Neutrophils expressing the high-affinity immunoglobulin-Fc receptor I (CD64) were described in numerous clinical studies over the last two decades (16). CD64 is normally expressed on monocytes, but its expression on circulating neutrophils could be due to its upregulation during inflammation (17), or to released immature granulocytes from the bone marrow, especially when it is associated with decreased expression of neutral endopeptidase (CD10) and low-affinity immuno-globulin-Fc fragment III (CD16) (13, 14, 18) (Supp.Tab.1) (19). Previous studies identified also the interleukin (IL)-3 as an orchestrator of emergency myelopoiesis during sepsis and showed its association with hospital mortality (20, 21). In

84  parallel, programmed death ligand-1 (PD-L1) expressed on monocytes was also described as a mortality-

85  predictor in sepsis patients (22, 23).

86  A systems-level view is likely needed to identify cellular features that specifically distinguish sepsis

87  infection-induced immune phenotypes from those triggered by aseptic inflammatory signals.  To identify

88  such early sepsis-specific cellular biomarkers, we developed a multi-parametric immune profiling strategy

89  (Fig.1). Cytometry by Time-Of-Flight (CyTOF) instrument was used to measure 42 markers on whole

90  blood immune cells from sepsis patients and controls (Fig.1A) (24). A computational analysis approach

91  was used to comprehensively characterize circulating immune cells and identify disease-specific cellular

92  signatures (25, 26). This approach consisted in a "discovery strategy" (Fig.1B) and a computational

93  "validation strategy" (Fig.1C) based on two complementary set of algorithms. We identified two

94  unreported early and sepsis-specific neutrophil subsets. A conventional "expert driven strategy" using a

95  limited set of markers confirmed that these two sepsis-specific neutrophil subsets were associated with

96  sepsis (Fig.1D). This result was confirmed using an independent cohort of patients and conventional flow

97  cytometry (Fig.1E).

98

99  **Methods**

100  *Study design*

101  This observational study was approved by the Comité de Protection des Personne Paris VII ethic

102  committee (CPP IDF VII A000142-53). Two cohorts were used in this study (Supp.Tab.2). Seventeen

103  sepsis (S) patients and twelve patients undergoing cardiac surgery considered as non-infected

104  inflammatory controls (NIC) were included in the discovery cohort of the study (Supp.Tab.2). The

105  validation cohort was composed of twenty-four sepsis patients and eighteen non-infected patients with

106 confoundable symptoms of sepsis (NIP) (Supp.Tab.2). Blood samples were drawn in heparin-coated

107 tubes, collected at the first- and seventh-day post admission of antibiotic treated sepsis patients or post-

108 surgery for NIC patients of the discovery cohort, and at the first-day post admission of the validation

109 cohort patients. In addition, blood samples of eleven age and gender matched healthy donors (HD)

110 were obtained from the French blood donation center. Five bone marrow (BM) biopsies from

111 orthopedic surgery patients were also included in this study.

112 *Mass cytometry analysis*

113 Whole blood samples were stained using a 42-dimensional mass cytometry panel (Supp.Tab.3). A

114 multi-step staining protocol was set up and is detailed in the supplementary methods section. Once the

115 collection of samples was completed, stained cells were thawed then measured on a CyTOF Helios

116 instrument. Acquired data were normalized with a MATLAB-based software (27) and analyzed using

117 the Cytobank platform (28).

118 *Computational data analysis*

119 To identify immune subsets and visualize all cells in a 2D map where position represents local phenotypic

120 similarity, we used two different dimensionality reduction tools depending on the strategy: the viSNE

121 implementation of t-SNE (29) and the UMAP (30). Cells were also grouped in phenotypically

122 homogenous clusters using either SPADE (31) or FlowSOM (32, 33). To phenotypically characterize

123 these clusters, Marker Enrichment Modeling (MEM) (34, 35) was used. The analysis process of each

124 strategy is detailed in the supplementary methods section.

125 *Flow cytometry validation panel*

126  To validate the sepsis-specific neutrophils signature a seven markers panel (Supp.Tab.4) was designed

127  for conventional florescent flow cytometry. The sepsis samples were analyzed in a blind cytometry

128  testing, along with the non-infected patients. The staining protocol is detailed in the supplementary

129  methods section.

130  *Activation and phagocytosis assay*

131  To address neutrophils activation and phagocytic capacities we used pHrodo-labeled BioParticles and

132  coated with *Staphylococcus aureus* (*S. aureus*) or Zymosan antigens (Invitrogen). The staining protocol

133  is detailed in the supplementary methods section.

134  *Statistical information*

135  Numerical data are given as median and inter-quartile range (25th - 75th percentile) with the exception

136  of Fig.7 data that are given as mean±SD. Nonparametric two-tailed Mann-Whitney test with a

137  significance threshold of alpha ($\alpha$=0.05) was used to compare cellular abundances of cell subsets

138  between two groups of patients and MFI ratios. Nonparametric two-tailed Wilcoxon signed-rank test

139  with a significance threshold of alpha ($\alpha$=0.05) was used to compare cellular abundances of cell subsets

140  from patients at day-1 and day-7. Relationship between two data sets was assessed using Spearman's

141  rank correlation coefficient (r) and test with a significance threshold of alpha ($\alpha$=0.05), and linear

142  regression line was drawn on the corresponding plot. Statistical tests were performed using GraphPad7

143  software (GraphPad Software, San Diego, CA), as well as receiver operator characteristic (ROC)

144  analyses.

145

146  **Results**

147 *Mass cytometry and computational analysis revealed a sepsis-specific neutrophil signature*

148 We designed a longitudinal observational study with 40 individuals to explore the evolution of circulating

149 immune cell phenotypes of S patients (n=17), NIC patients (n=12) at day 1 and 7 (Supp.Tab.2) and HD

150 (n=11) in addition to BM biopsies (n=5) (Fig.1A). Whole blood immunostaining was performed with a

151 42-parameter mass cytometry panel designed to give a comprehensive evaluation of circulating leukocytes

152 (Fig.1A, Supp.Tab.3). We identified circulating immune cell populations. Using viSNE tool, neutrophils

153 were gated, and other circulating immune cells were independently analyzed.

154 The neutrophils were analyzed with a "discovery strategy" using viSNE and SPADE tools (Fig.1B).

155 viSNE is an unsupervised algorithm that reduces feature dimensions and allows cells visualization in a

156 two-dimensional map. SPADE is an unsupervised algorithm aiming to group cells into nodes that could

157 be displayed on the viSNE map. This strategy allowed to define an imprint for each sample group

158 (Fig.2A). On the resulting map, neutrophils of S and NIC day-1 patients and neutrophils of HD were

159 arranged in three different areas (Fig.2A). These S neutrophils were clustered in specific nodes that were

160 absent from NIC and HD (Supp.Fig.1, 2). Some of these S specific nodes were shared with BM,

161 suggesting the occurrence of myelocytosis for S patients (Supp.Fig.1, 2). Most cells from day-7 samples

162 were phenotypically similar to samples from HD (Fig.2A, Supp.Fig.1, 2). CD16, CD10 and CD64

163 markers split neutrophils signature into two positive and negative subpopulations for each marker

164 (Supp.Fig.1). To characterize all the nodes, their abundance in each sample and their average expression

165 of each marker were extracted and used to generate two heatmaps (Supp.Fig.3, 4). Hierarchical clustering

166 was used to arrange rows (nodes) and columns (samples) of the frequency heatmap (Supp.Fig.3) and

167 columns (markers) of the phenotype heatmap (Supp.Fig.4). In this unsupervised three arms analysis

168 (nodes, samples and markers), the resulting dendrograms led to the identification of 3 main samples

169 clusters (columns) as shown in Fig2B (Supp.Fig.3 before tree cut). Most of the samples were clustered

according to patient groups. S day-1 (pink) and BM (orange) samples were clustered together. S day-7 samples were split in two sample clusters, with half of them clustering with HD samples (Fig2B, Supp.Fig.3) suggesting the acquisition of a "healthy" neutrophil phenotype profile (Fig2A). In addition, this unsupervised strategy allowed the precise delimitation of four groups of cell nodes (Fig.2D): [1] HD-abundant nodes representing neutrophils with $CD16^{high}CD10^{med}CD64^-$ phenotype, [2] NIC and S day-7 common nodes harboring $CD16^+CD10^{med}CD64^-$ phenotype, [3] day-1 NIC and S common nodes defined as $CD16^{low}CD10^-CD64^{low}$, and [4] S day-1 and BM nodes with $CD10^-CD64^+$ phenotype. Node group [4] represents cells that are highly abundant in sepsis samples at day-1 when compared to other patient groups (Supp.Fig.5A). The statistical analyses of these nodes are presented in Supp.Fig.5B. Among the nodes that statistically discriminate S and NIC at day-1 (Supp.Fig.5B), a specific phenotypic characteristic was observed: three nodes expressed CD123 and four other nodes expressed PD-L1 (Supp.Fig.5A, Fig.2C, D). On the basis of phenotypic homogeneity meta-clusters were generated to group nodes that share similar expression of these two markers and represent two neutrophil subsets specific to S at day-1 and observed to be lacking in NIC neutrophils (Fig.2E). The first subset (in red) was composed of $CD10^-CD64^+CD16^+PD-L1^+$ neutrophils (S median proportion: 18.08 (6.69-48.33) %, NIC median proportion: 0.81 (0.53-3.01) %, *p=0.0002*) and the second one (in blue) identified as $CD10^-CD64^+CD16^{low}CD123^+$ immature neutrophils (S median proportion: 10.06 (1.12-39.35) %, NIC median proportion: 0.04 (0.02-0.42) %, *p<0.0001*) (Fig.2E). We also recapitulated previously described results (13, 14, 18) regarding the sepsis related increase of circulating immature $CD10^-CD64^+$ neutrophils when compared to NIC at day-1 (S median proportion: 11.03 (1.41-40.39) %, NIC median proportion: 0.62 (0.12-1.46) %, *p=0.001*) and we confirmed their phenotypic similarities with a third of BM neutrophils (BM median proportion: 37.39 (17.90-46.48) %) (Fig.2E). Also, we noticed that all HD specific-nodes were absent in S patient day-1 samples (Fig.2B, D).

193 With this strategy, two novel neutrophil subsets were identified, including CD123$^+$ cells (red) and PD-

194 L1$^+$ cells (blue), and the absence of HD neutrophil phenotypes at an early stage of sepsis.

195 *A computational validation strategy confirmed sepsis day-1 specific neutrophil subsets*

196 To test whether the previously identified neutrophil subsets were sepsis-specific and robust, an

197 independent unsupervised data analysis strategy was applied on the same data files used in the discovery

198 strategy (Fig.1B, C). This "validation strategy" was based on UMAP and FlowSOM algorithms. UMAP

199 is an unsupervised dimensional reduction algorithm (Supp.Fig.6A) and FlowSOM is an unsupervised

200 clustering algorithm. This strategy allowed the identification of 50 neutrophil clusters and the complete

201 linkage hierarchical clustering of their relative cell abundance arranged again the samples according to

202 patient groups (Supp.Fig.6B). Two main cell cluster groups (pink gates) appeared to be more abundant

203 in sepsis samples (Supp.Fig.6B, C) and almost all HD associated-clusters (purple gate) were absent in

204 sepsis patient day-1 samples.

205 To phenotypically characterize the pink gate clusters, MEM phenotype annotation tool was used. The

206 MEM label of each cluster is an objective description of what makes that subset distinct from all the other

207 clusters. Among these clusters, three cell meta-clusters were identified, one with CD10$^-$CD64$^+$ immature

208 cells (pink clusters), and two meta-clusters phenotypically identical to the "discovery strategy" sepsis-

209 specific neutrophils nodes (Supp.Fig.6D, Fig.3A). Red clusters contained CD10$^-$CD64$^+$PD-L1$^+$

210 neutrophils with a median cell proportion of 5.50 (1.15-38.03) % for S day-1 samples and 0.09 (0.02-

211 0.33) % for NIC day-1 samples (*p<0.0001*) (Fig.3B). Blue clusters gathered CD10$^-$CD64$^+$CD16$^{low/-}$

212 CD123$^+$ immature neutrophils with median cell proportions of 2.43 (0.98-6.32) % and 0.04 (0.03-0.28)

213 % for S day-1 and NIC day-1 samples respectively (*p=0.0006*) (Fig.3B). We also visually noted that red

214 clusters (PD-L1$^+$ cells) and blue clusters (CD123$^+$ cells) from the "validation strategy" are co-localized

8

215    with red nodes (PD-L1$^+$ cells) and blue nodes (CD123$^+$ cells), respectively, from the "discovery strategy",

216    when back mapped onto the t-SNE1-2/t-SNE2-2 axes (Fig.3C).

217    *Expert gating strategy based on a limited set of markers validated the sepsis day-1 neutrophil signature*

218    *that correlates with SAPSII and SOFA scores*

219    After cell subsets were identified by automatic and high-dimensional analysis strategies, we determined

220    whether the identified neutrophil signature could be found using conventional analysis applicable by

221    experts. The use of such gating strategy would make it easier to transpose it to clinical use.

222    A bi-parametric gating strategy on a limited set of markers allowed the identification of neutrophils

223    expressing CD123 and PD-L1 (Fig.4A). When CD123$^+$ and PD-L1$^+$ sepsis-specific neutrophils were

224    mapped back onto both t-SNE1-2/t-SNE2-2 axes and UMAP1/UMAP2 axes, they located in the same

225    regions as the cells identified by the two previous computational strategies meaning that they share the

226    same phenotype (Fig.4A). This expert gating strategy applied on the current dataset, allowed the selection

227    of PD-L1 expressing neutrophils that were significantly more abundant in blood of S day-1 patients (9.25

228    (3.61-36.97) %) when compared to NIC day-1 patients (0.12 (0.07- 0.60) %, p<0.0001) or HD (0.01 (0.00-

229    0.03) %, p<0.001) (Fig.4B). Similarly, expert gating allowed the selection of S-specific neutrophils (2.47

230    (0.44-17.42) %) that were consistent with CD123$^+$ red subsets cells phenotype and that were almost absent

231    from NIC (0.04 (0.07-0.87) %, p<0.0001) or HD (0.04 (0.02-0.10) %, p<0.0001) (Fig.4B).

232    Although the proportion of CD10-CD64+CD16-CD123+ neutrophils could distinguish S and NIC

233    samples at day 1, we observed a large variability between patients. Interestingly, we noticed that patients

234    with the highest CD123+ neutrophil subset proportion (> 20%) tended to be more severe (requirement for

235    mechanical ventilation and catecholamine support). Later correlation with severity scores confirmed this

236    observation. The proportion of CD123$^+$ sepsis-specific, assessed by the simple gating strategy on mass

237  cytometry data, positively correlated with Simplified Acute Physiology Score II (SAPS II) (Spearman

238  r=0.62, *p*=0.0192) and Sequential Organ Failure Assessment (SOFA) score (Spearman r=0.55, *p*=0.0437)

239  (Fig.4C). However, the proportion of CD123+ neutrophil was not influenced by sepsis endotype. The

240  proportions of PD-L1 neutrophil subset did not correlate with severity scores nor sepsis endotypes. ROC

241  analysis of these CD123+ neutrophils abundance was carried out to determine the optimal threshold

242  separating sepsis patients from non-infected patients. A cut-off point of 0.38% of the CD123+ neutrophil

243  subset abundance was able to identify sepsis patients with a specificity of 91.67% and sensitivity of

244  81.25% and display an area under the ROC curve (AUROC) of 0.91 (Fig.4D). When combining the

245  abundance of the CD123+ and PD-L1+ neutrophil subsets, the cut-off point changed to 0.93% and lowered

246  both the sensitivity, to 75%, and the specificity, to 83.33%. (Fig.4E). Whereas a clinical SOFA score >2

247  was discriminating with a good sensitivity (94.12%) but with a poor specificity (45.45%) and a worst

248  AUROC of 0.79 (Fig.4F). In addition, the AUROC of SAPS-II score was also lower (AUROC=0.82) with

249  a sensitivity of 88.24% and a poor specificity of 45.45% (Fig.4G).

250  Thus, a simple gating strategy assessing only 7 key markers identified successfully CD123+ and PD-L1+

251  sepsis-specific neutrophils and indicated that CD123+ neutrophils may be a marker of sepsis severity with

252  a better discriminating efficiency when compared to clinical scores.

253  *Mass cytometry and unsupervised analysis identified classical sepsis immune hallmarks*

254  Using two complementary computational strategies, we identified a sepsis-specific signature on the

255  neutrophil cells. We asked whether a signature in the non-neutrophil cells could reinforce the CD123$^+$ and

256  PD-L1$^+$ neutrophil subsets as sepsis biomarker candidates. The non-neutrophils circulating immune cells

257  were computationally analyzed using t-SNE and SPADE algorithms. A heatmap was generated to

258  characterize nodes phenotype and to delimitate the main circulating non-neutrophil immune cell

259 populations, according to complete linkage hierarchical clustering (Supp.Fig.7A). These populations

260 were then color coded and backgated on the t-SNE map (Supp.Fig.7B). Classical hallmarks of sepsis were

261 identified, including lymphopenia, monocytopenia and a persistent lower level of monocytes HLA-DR in

262 S patients when compared to HD group ($p<0.0001$, $p=0.0426$ and $p<0.0001$ respectively, Fig.5A). In

263 parallel, we observed an elevated number of circulating neutrophils $(p=0.0039)$, and consistent with that,

264 a higher neutrophil to lymphocyte ratio ($p<0.0001$) in S vs. HD (Fig.5B). These trends were not exclusive

265 to S, but were also observed in NIC group when compared to HD group ($p=0.0003$, $p<0.0001$, $p=0.0034$,

266 $p<0.0001$, for lymphocytes and neutrophils counts, monocytes HLA-DR expression level and

267 neutrophils/lymphocytes ratio, respectively). No significant difference was observed between S and NIC

268 group at day-1 within these main immune cell populations (Supp.Tab.2).

269 To identify an early sepsis-specific signature within these immune populations, we compared the

270 abundance of the identified cell nodes of these immune populations between HD, NIC and S samples at

271 day-1. The abundance of 22 nodes was found selectively regulated in S at day-1 when compared to both

272 NIC and HD and 25 nodes differentiated S only from NIC at day-1 (Supp.Fig.7C, D). It included notably

273 15 nodes identifying classical monocytes with high expression of HLD-DR, 3 nodes of CD4$^+$ T

274 lymphocytes and CD8$^+$ T lymphocytes expressing CCR2 and CCR6, all were highly reduced in S patients,

275 one node of B lymphocytes with a low expression of B cells pan markers (HLD-DR, CXCR5, CD19 and

276 CCR6) and one node identified monocyte-derived DC (Fig.5C). Among the nodes that were massively

277 reduced in both S and NIC sample, 15 nodes out of 55 represent Basophils and Eosinophils subsets

278 (Fig.5D); the others being scattered among other cell populations.

279 Taken globally, the analysis of circulating non-neutrophil cells with a computational strategy allowed us

280 to resume sepsis hallmarks and identify the differences of several circulating immune subsets abundance.

*CD123+ and PD-L1+ sepsis-specific neutrophils are detectable by conventional cytometry and discriminate infected and non-infected patients*

We identified two neutrophil subsets using 40 individuals and 42-marker mass cytometer and computational analysis. These subsets might be detectable by conventional cytometry approach that is used in routine in the clinic. To evaluate the efficiency and specificity of CD123$^+$ and PD-L1$^+$ neutrophil subsets to discriminate sepsis patients from non-infected ones, we set up a fluorescent 7-marker flow cytometry panel (Supp.Tab.4). We monitored an independent validation cohort composed of non-infected patients (n=18) and sepsis patients (n=24).

With the overlay of full minus-two (FMT) stained control and the full panel stained tubes of three representative patients of several expression levels of CD10, CD123 and PDL1, we appreciated the increase of CD123$^+$ and PD-L1$^+$ sepsis-specific neutrophil subsets with the decrease of CD10 expression by neutrophils (CD14$^-$CRTH2$^-$CD15$^+$ cells) (Fig.6A). ROC analysis was performed using CD123$^+$ and PD-L1$^+$ neutrophil subsets abundances, measured by conventional flow cytometry on an independent validation cohort of sepsis and non-infected patients. A cut-off point of 0.35% of the CD123$^+$ neutrophil subset abundance was able to rule out sepsis patients with a specificity of 94.44% and sensitivity of 87.5% and an AUROC of 0.95 (Fig.6B). When combining the abundance of the CD123$^+$ and PD-L1$^+$ neutrophil subsets, the cut-off point changed to 0.60% with no effect on the sensitivity nor on the specificity (Fig.6C). Whereas, a clinical SOFA score >2 was discriminating with a good sensitivity (91.30%) but with a poor specificity (18.18%) and a worst AUROC of 0.61 (Fig.6D). In addition, the AUROC of SAPS-II score was also lower (AUROC=0.69) with a sensitivity of 91.67% and a poor specificity of 25.00% (Fig.6E). These results indicated that conventional flow cytometry recapitulates the results obtained by mass cytometry and confirmed that the identified neutrophil subsets could be a marker of sepsis severity with

303 a better efficiency than clinical scores and reliably quantified by routinely performed clinical flow

304 cytometric profiling

305 In addition, we evaluated if the CD123+ neutrophil subset was only abundant in patients with the highest

306 severity scores. We used the data generated in both the discovery (Fig.4) and the validation cohorts (Fig.6)

307 and divided the cohorts by quartile of severity according to SOFA and SAPS II scores (Supp.Fig.8A, B).

308 While sepsis and non-infected patients overlap greatly their severity scores, the proportion of CD123+

309 neutrophils subset distinguishes efficiently sepsis and control groups in both discovery (Supp.Fig.8A) and

310 validation cohorts (Supp.Fig.8B).

311 *Immature sepsis neutrophils exhibit an impaired microbial specific activation and phagocytosis*

312 To address sepsis-associated neutrophils activation and phagocytic capacities, whole blood of each tested

313 individual was incubated with *Staphylococcus aureus* (*S. aureus*) or Zymosan coated bio-particles labelled

314 with pHrodo, a pH-sensitive fluorochrome (36), in order to identify immature neutrophils bio-particles

315 uptake capacity and activation.

316 All immature circulating neutrophils (CD64+CD10⁻) were able to phagocyte *Staphylococcus aureus* (*S.*

317 *aureus*) beads independently from their group (HD, S-D1, BM). However, S day-1 neutrophils

318 phagocytosis of Zymosan Beads (Mean±SD=28.12±8.39%) was not as effective as that of HD

319 (Mean±SD=50.43±13.04, $p$=0.02) (Fig.7A). This sepsis-associated decrease of phagocytosis goes with

320 the proportion increase of both CD123+ and PD-L1+ immature neutrophil subsets in the blood of the

321 tested sepsis patients when compared to HD (Fig.7B). t-SNE visualization of PC and NC neutrophils of

322 both *S. aureus* (Fig.7C, D) and Zymosan (Fig.7E, F) bead stimulations highlighted the lower expression

323 level of CD11b marker by S day-1 neutrophils when compared to HD and the default of activation of

324 these cells after microbial beads activation. In fact, S neutrophils exhibited a lower ratio of CD11b and

325 CD66b MFI between PC and NC after activation, when compared to healthy donors after *S. aureus*

326 (Fig.7D) or Zymosan (Fig.7F) stimulations. The impaired phagocytic capacity of sepsis-patients'

327 immature neutrophils compared to HD neutrophils was confirmed by the measurement of phagocytosed

328 beads MFI ratios between PC and NC. This ratio was three times lower for S day-1 *S. aureus* response

329 (Fig.7D) and 30% lower for S day-1 Zymosan response (Fig.7F). These data allowed the identification

330 of an impaired capacity of immature sepsis neutrophils to form efficient phagolysosomes after bio-

331 particles stimulation and a default of activation when compared to HD.

332

**333 Discussion**

334 Whole blood mass cytometry and computational analysis identified classical hallmarks of sepsis, and

335 revealed two novel neutrophil subsets that distinguish early sepsis from aseptic inflammatory

336 syndromes. Two novel neutrophil subsets were identified, CD10$^-$CD64$^+$PD-L1$^+$ neutrophils and CD10$^-$

337 CD64$^+$CD16$^{low/-}$CD123$^+$ immature neutrophils that could be used for early identification of sepsis

338 patients. CD123+ and PDL1+ neutrophil subsets could help improving sepsis diagnosis and guide sepsis

339 treatment monitoring.

340 The results of this study recapitulated previous original findings and meta-analysis studies regarding the

341 sepsis-related increase of circulating immature CD10$^-$CD64$^+$ neutrophils (13, 14, 18, 37). Despite all these

342 large efforts, the CD64 detection-based tools are not yet standardized for sepsis diagnosis, because of the

343 heterogeneity of sepsis syndrome and inter-individual variability of CD64 basal level among sepsis

344 patients.

345 The CD10$^-$CD64$^+$CD16$^{low/-}$CD123$^+$ population is most consistent with immature neutrophils. The

346 frequency of this population among total neutrophils positively correlates with both SAPS II and SOFA

347 severity scores, and need to be confirmed in a larger collection. The neutrophils expression of CD123 was

348 not described before during sepsis. In a previous study of Weber *et al.,* using a mouse model of abdominal

349 sepsis, the cytokine IL-3 was reported to potentiate inflammation in sepsis by inducing myelopoiesis of

350 neutrophils and IL-3 deficiency protects mice against sepsis (20). Moreover, the authors described an

351 association between high plasma IL-3 levels and high mortality. This result was also obtained in a recent

352 prospective cohort study, where higher levels of IL-3 were shown to be independently associated with

353 hospital mortality in septic patients (21). All these results identify IL-3 and its receptor CD123 as an

354 orchestrator of emergency myelopoiesis, and reveals a new target for the diagnosis and treatment of sepsis.

355 To our knowledge, the expression of PD-L1 by neutrophil during sepsis was not reported before. It was

356 defined on monocytes, macrophages and endothelial cells (38) but not granulocytes. Monocyte PD-L1

357 expression was described as an independent predictor of 28-day mortality in patients with septic shock

358 (22, 23). Peripheral blood transcriptomic analysis done by Uhle *et al*., revealed the expression of PD-L1-

359 gene among the top 44 immune-related genes differentially expressed between patients with sepsis and

360 healthy donors (15). In parallel, mice in which the PD-1/PD-L1 interaction was inhibited show improved

361 survival to sepsis (39). Our results bring up a new target for the immune checkpoint therapies.

362 Controversial results were previously described regarding functional aspects of neutrophils during sepsis.

363 On one hand, Demaret *et al*., described conserved phagocytosis and activation capacities of sepsis

364 neutrophils characterized as CD10$^{dim}$CD16$^{dim}$ immature cells, after whole blood IL8, fMLP or FITC-

365 labeled *Escherichia coli* stimulation cells (40). On the other hand, Drifte *et al*., by comparing mature and

366 immature neutrophils functions found that the latter were less efficient in phagocytosis and killing.

367 Accordingly, we observed an impaired capacity of cells to form efficient phagolysosomes after bio-

368 particles stimulation and a default of activation when compared to HD.

369 The immunosuppressive function was also attributed to G-MDSC neutrophils subset during sepsis (13-

370 15, 18). But, to date, human G-MDSC definition lacks consensual phenotypic characterization.

371 Published results on G-MDSC in cancer were obtained according to various phenotypes. Condamine

372 *et al.* described them as Lectin-type oxidized LDL receptor-1 (LOX1) expressing cells (41). Using

373 flow cytometry, we measured the expression of LOX-1 in sepsis patients (data not shown). No LOX-

374 1 co-staining was observed with neither CD123^{+} nor PD-L1^{+} subsets. More investigation is needed to

375 characterize if CD123^{+} neutrophils and PD-L1^{+} subset belong to G-MDSC.

376 Further research should be conducted to identify appropriate clinical actions for each identified

377 neutrophil subset and their evolution over time course and in different cohorts of patients

378 (undifferentiated shock patients, immunosuppressed patients, different types of infections, durability

379 of neutrophil population after antibiotics), to understand whether altered neutrophil production is

380 responsible for increased sepsis risk, and to determine how these subsets can be therapeutically

381 targeted.

382 In this study we show that the use of the identified neutrophil subsets gives complementary information

383 to severity scores such as SOFA and SAPS II and are specific of sepsis. In the discovery cohort, in

384 which stringent selection was applied for sepsis and non-infected control patient inclusion, few

385 differences were observed between AUROC of CD123+ neutrophils, SOFA and SAPS II scores (Fig.

386 4D, F, G). In contrast, the validation cohort, where blind analysis was performed, SOFA and SAPS II

387 lose their discrimination power (Fig. 6D, E) and CD123+ neutrophils biomarker remain highly specific

388 and sensitive for sepsis patient identification.

389 In addition, the diagnosis of sepsis was evoked for a significant proportion of patients (6/18) in the

390 ICU control group of the validation cohort, a third of them received antibiotics due to their clinical

391 characteristics but the diagnosis of sepsis was finally dropped out. They ended to be non-infected and

392 undistinguishable from other inflamed and non-infected controls (Supp.Tab.5). Of note, the CD123+

393 neutrophils proportion of these patients was <0.3%, below the cutoff value identified in our ROC

394 analysis. The use of this biomarker candidate would have avoided this unnecessary administration of

395 antibiotics. Especially that flow cytometry is a widely available technique in the clinic, with reasonable

396 costs and results can be rapidly obtained.

397 The use of a whole blood flow cytometry test to diagnose sepsis could change the fate of patient's care.

398 The clinician would have a rapid and specific result, obtained before microbiological cultures results,

399 that could guide their therapeutic decision.

400 In parallel, future studies should now be undertaken to validate the use of these new neutrophil subsets

401 in clinic by routine flow cytometry as an early biomarker predictive of sepsis. Larger cohorts that better

402 represent not only sepsis patients but also the diversity of aseptic inflammatory syndromes need to be

403 evaluated.

404 Delay to sepsis diagnosis has been shown to decrease survival and increase hospital costs, a better

405 diagnosis will definitely help to improve patient's care, avoid unnecessary treatments and reduce

406 hospital length of stay.

407

412

**References**

1. Seymour CW, Liu VX, Iwashyna TJ, Brunkhorst FM, Rea TD, Scherag A, Rubenfeld G, Kahn JM, Shankar-Hari M, Singer M, Deutschman CS, Escobar GJ, Angus DC. Assessment of Clinical Criteria for Sepsis: For the Third International Consensus Definitions for Sepsis and Septic Shock (Sepsis-3). *Jama* 2016; 315: 762-774.

2. Fleischmann C, Scherag A, Adhikari NK, Hartog CS, Tsaganos T, Schlattmann P, Angus DC, Reinhart K. Assessment of Global Incidence and Mortality of Hospital-treated Sepsis. Current Estimates and Limitations. *American journal of respiratory and critical care medicine* 2016; 193: 259-272.

3. Hotchkiss RS, Moldawer LL, Opal SM, Reinhart K, Turnbull IR, Vincent JL. Sepsis and septic shock. *Nature reviews Disease primers* 2016; 2: 16045.

4. Yang Y, Xie J, Guo F, Longhini F, Gao Z, Huang Y, Qiu H. Combination of C-reactive protein, procalcitonin and sepsis-related organ failure score for the diagnosis of sepsis in critical patients. *Annals of intensive care* 2016; 6: 51.

5. Moreno R, Vincent JL, Matos R, Mendonça A, Cantraine F, Thijs L, Takala J, Sprung C, Antonelli M, Bruining H, Willatts S. The use of maximum SOFA score to quantify organ dysfunction/failure in intensive care. Results of a prospective, multicentre study. Working

440   Group on Sepsis related Problems of the ESICM. *Intensive care medicine* 1999; 25: 686-
441   696.

442   6. Wasserman A, Karov R, Shenhar-Tsarfaty S, Paran Y, Zeltzer D, Shapira I, Trotzky D,
443   Halpern P, Meilik A, Raykhshtat E, Goldiner I, Berliner S, Rogowski O. Septic patients
444   presenting with apparently normal C-reactive protein: A point of caution for the ER
445   physician. *Medicine (Baltimore)* 2019; 98: e13989.

446   7. Minne L, Abu-Hanna A, de Jonge E. Evaluation of SOFA-based models for predicting
447   mortality in the ICU: A systematic review. *Critical care (London, England)* 2008; 12:
448   R161.

449   8. Singer M, Deutschman CS, Seymour CW, Shankar-Hari M, Annane D, Bauer M, Bellomo R,
450   Bernard GR, Chiche JD, Coopersmith CM, Hotchkiss RS, Levy MM, Marshall JC, Martin
451   GS, Opal SM, Rubenfeld GD, van der Poll T, Vincent JL, Angus DC. The Third
452   International Consensus Definitions for Sepsis and Septic Shock (Sepsis-3). *Jama* 2016;
453   315: 801-810.

454   9. Kumar A, Roberts D, Wood KE, Light B, Parrillo JE, Sharma S, Suppes R, Feinstein D,
455   Zanotti S, Taiberg L, Gurka D, Kumar A, Cheang M. Duration of hypotension before
456   initiation of effective antimicrobial therapy is the critical determinant of survival in
457   human septic shock. *Critical care medicine* 2006; 34: 1589-1596.

458   10. van der Poll T, van de Veerdonk FL, Scicluna BP, Netea MG. The immunopathology of
459   sepsis and potential therapeutic targets. *Nature reviews Immunology* 2017; 17: 407-420.

460   11. Treacher DF, Sabbato M, Brown KA, Gant V. The effects of leucodepletion in patients who
461   develop the systemic inflammatory response syndrome following cardiopulmonary
462   bypass. *Perfusion* 2001; 16 Suppl: 67-73.

463   12. Brown KA, Brain SD, Pearson JD, Edgeworth JD, Lewis SM, Treacher DF. Neutrophils in
464   development of multiple organ failure in sepsis. *Lancet (London, England)* 2006; 368:
465   157-169.

466   13. Daix T, Guerin E, Tavernier E, Mercier E, Gissot V, Herault O, Mira JP, Dumas F, Chapuis
467   N, Guitton C, Bene MC, Quenot JP, Tissier C, Guy J, Piton G, Roggy A, Muller G, Legac
468   E, de Prost N, Khellaf M, Wagner-Ballon O, Coudroy R, Dindinaud E, Uhel F, Roussel
469   M, Lafon T, Jeannet R, Vargas F, Fleureau C, Roux M, Allou K, Vignon P, Feuillard J,

470            Francois B. Multicentric Standardized Flow Cytometry Routine Assessment of Patients
471            With Sepsis to Predict Clinical Worsening. *Chest* 2018; 154: 617-627.

472 14. Guerin E, Orabona M, Raquil MA, Giraudeau B, Bellier R, Gibot S, Bene MC, Lacombe F,
473            Droin N, Solary E, Vignon P, Feuillard J, Francois B. Circulating immature granulocytes
474            with T-cell killing functions predict sepsis deterioration*. *Critical care medicine* 2014;
475            42: 2007-2018.

476 15. Uhel F, Azzaoui I, Gregoire M, Pangault C, Dulong J, Tadie JM, Gacouin A, Camus C,
477            Cynober L, Fest T, Le Tulzo Y, Roussel M, Tarte K. Early Expansion of Circulating
478            Granulocytic Myeloid-derived Suppressor Cells Predicts Development of Nosocomial
479            Infections in Patients with Sepsis. *American journal of respiratory and critical care*
480            *medicine* 2017; 196: 315-327.

481 16. Mahmoodpoor A, Paknezhad S, Shadvar K, Hamishehkar H, Movassaghpour AA, Sanaie S,
482            Ghamari AA, Soleimanpour H. Flow Cytometry of CD64, HLA-DR, CD25, and TLRs for
483            Diagnosis and Prognosis of Sepsis in Critically Ill Patients Admitted to the Intensive Care
484            Unit: A Review Article. *Anesthesiology and pain medicine* 2018; 8: e83128.

485 17. Barth E, Fischer G, Schneider EM, Wollmeyer J, Georgieff M, Weiss M. Differences in the
486            expression of CD64 and mCD14 on polymorphonuclear cells and on monocytes in
487            patients with septic shock. *Cytokine* 2001; 14: 299-302.

488 18. Bae MH, Park SH, Park CJ, Cho EJ, Lee BR, Kim YJ, Park SH, Cho YU, Jang S, Song DK,
489            Hong SB. Flow cytometric measurement of respiratory burst activity and surface
490            expression of neutrophils for septic patient prognosis. *Cytometry Part B, Clinical*
491            *cytometry* 2016; 90: 368-375.

492 19. Elghetany MT. Surface antigen changes during normal neutrophilic development: a critical
493            review. *Blood cells, molecules & diseases* 2002; 28: 260-274.

494 20. Weber GF, Chousterman BG, He S, Fenn AM, Nairz M, Anzai A, Brenner T, Uhle F,
495            Iwamoto Y, Robbins CS, Noiret L, Maier SL, Zonnchen T, Rahbari NN, Scholch S,
496            Klotzsche-von Ameln A, Chavakis T, Weitz J, Hofer S, Weigand MA, Nahrendorf M,
497            Weissleder R, Swirski FK. Interleukin-3 amplifies acute inflammation and is a potential
498            therapeutic target in sepsis. *Science (New York, NY)* 2015; 347: 1260-1265.

499 21. Borges IN, Resende CB, Vieira ELM, Silva J, Andrade MVM, Souza AJ, Badaro E, Carneiro
500   RM, Teixeira AL, Jr., Nobre V. Role of interleukin-3 as a prognostic marker in septic
501   patients. *Revista Brasileira de terapia intensiva* 2018; 30: 443-452.
502 22. Shao R, Fang Y, Yu H, Zhao L, Jiang Z, Li CS. Monocyte programmed death ligand-1
503   expression after 3-4 days of sepsis is associated with risk stratification and mortality in
504   septic patients: a prospective cohort study. *Critical care (London, England)* 2016; 20:
505   124.
506 23. Tai H, Xing H, Xiang D, Zhu Z, Mei H, Sun W, Zhang W. Monocyte Programmed Death
507   Ligand-1, A Predicator for 28-Day Mortality in Septic Patients. *The American journal of*
508   *the medical sciences* 2018; 355: 362-367.
509 24. Bendall SC, Simonds EF, Qiu P, Amir el AD, Krutzik PO, Finck R, Bruggner RV, Melamed
510   R, Trejo A, Ornatsky OI, Balderas RS, Plevritis SK, Sachs K, Pe'er D, Tanner SD, Nolan
511   GP. Single-cell mass cytometry of differential immune and drug responses across a
512   human hematopoietic continuum. *Science (New York, NY)* 2011; 332: 687-696.
513 25. Greenplate AR, Johnson DB, Ferrell PB, Jr., Irish JM. Systems immune monitoring in cancer
514   therapy. *European journal of cancer* 2016; 61: 77-84.
515 26. Irish JM. Beyond the age of cellular discovery. *Nature immunology* 2014; 15: 1095-1097.
516 27. Finck R, Simonds EF, Jager A, Krishnaswamy S, Sachs K, Fantl W, Pe'er D, Nolan GP,
517   Bendall SC. Normalization of mass cytometry data with bead standards. *Cytometry Part A*
518   *: the journal of the International Society for Analytical Cytology* 2013; 83: 483-494.
519 28. Kotecha N, Krutzik PO, Irish JM. Web-based analysis and publication of flow cytometry
520   experiments. *Current protocols in cytometry* 2010; Chapter 10: Unit10.17.
521 29. Amir el AD, Davis KL, Tadmor MD, Simonds EF, Levine JH, Bendall SC, Shenfeld DK,
522   Krishnaswamy S, Nolan GP, Pe'er D. viSNE enables visualization of high dimensional
523   single-cell data and reveals phenotypic heterogeneity of leukemia. *Nature biotechnology*
524   2013; 31: 545-552.
525 30. Becht E, McInnes L, Healy J, Dutertre CA, Kwok IWH, Ng LG, Ginhoux F, Newell EW.
526   Dimensionality reduction for visualizing single-cell data using UMAP. *Nature*
527   *biotechnology* 2018.

528    31. Qiu P, Simonds EF, Bendall SC, Gibbs KD, Jr., Bruggner RV, Linderman MD, Sachs K,
529        Nolan GP, Plevritis SK. Extracting a cellular hierarchy from high-dimensional cytometry
530        data with SPADE. *Nature biotechnology* 2011; 29: 886-891.
531    32. Van Gassen S, Callebaut B, Van Helden MJ, Lambrecht BN, Demeester P, Dhaene T, Saeys
532        Y. FlowSOM: Using self-organizing maps for visualization and interpretation of
533        cytometry data. *Cytometry Part A : the journal of the International Society for Analytical*
534        *Cytology* 2015; 87: 636-645.
535    33. Leelatian N, Sinnaeve J, Mistry AM, Barone SM, Diggins KE, Greenplate AR, Weaver KD,
536        Thompson RC, Chambless LB, Mobley BC, Ihrie RA, Irish JM. High risk glioblastoma
537        cells revealed by machine learning and single cell signaling profiles. *bioRxiv* 2019:
538        632208.
539    34. Diggins KE, Gandelman JS, Roe CE, Irish JM. Generating Quantitative Cell Identity Labels
540        with Marker Enrichment Modeling (MEM). *Current protocols in cytometry* 2018; 83:
541        10.21.11-10.21.28.
542    35. Diggins KE, Greenplate AR, Leelatian N, Wogsland CE, Irish JM. Characterizing cell subsets
543        using marker enrichment modeling. *Nature methods* 2017; 14: 275-278.
544    36. Neaga A, Lefor J, Lich KE, Liparoto SF, Xiao YQ. Development and validation of a flow
545        cytometric method to evaluate phagocytosis of pHrodo BioParticles(R) by granulocytes in
546        multiple species. *Journal of immunological methods* 2013; 390: 9-17.
547    37. Wang X, Li ZY, Zeng L, Zhang AQ, Pan W, Gu W, Jiang JX. Neutrophil CD64 expression as
548        a diagnostic marker for sepsis in adult patients: a meta-analysis. *Critical care (London,*
549        *England)* 2015; 19: 245.
550    38. Boomer JS, To K, Chang KC, Takasu O, Osborne DF, Walton AH, Bricker TL, Jarman SD,
551        2nd, Kreisel D, Krupnick AS, Srivastava A, Swanson PE, Green JM, Hotchkiss RS.
552        Immunosuppression in patients who die of sepsis and multiple organ failure. *Jama* 2011;
553        306: 2594-2605.
554    39. Huang X, Venet F, Wang YL, Lepape A, Yuan Z, Chen Y, Swan R, Kherouf H, Monneret G,
555        Chung CS, Ayala A. PD-1 expression by macrophages plays a pathologic role in altering
556        microbial clearance and the innate inflammatory response to sepsis. *Proceedings of the*
557        *National Academy of Sciences of the United States of America* 2009; 106: 6303-6308.

558    40. Demaret J, Venet F, Friggeri A, Cazalis MA, Plassais J, Jallades L, Malcus C, Poitevin-Later

559        F, Textoris J, Lepape A, Monneret G. Marked alterations of neutrophil functions during

560        sepsis-induced immunosuppression. *Journal of leukocyte biology* 2015; 98: 1081-1090.

561    41. Condamine T, Dominguez GA, Youn JI, Kossenkov AV, Mony S, Alicea-Torres K,

562        Tcyganov E, Hashimoto A, Nefedova Y, Lin C, Partlova S, Garfall A, Vogl DT, Xu X,

563        Knight SC, Malietzis G, Lee GH, Eruslanov E, Albelda SM, Wang X, Mehta JL, Bewtra

564        M, Rustgi A, Hockstein N, Witt R, Masters G, Nam B, Smirnov D, Sepulveda MA,

565        Gabrilovich DI. Lectin-type oxidized LDL receptor-1 distinguishes population of human

566        polymorphonuclear myeloid-derived suppressor cells in cancer patients. *Science*

567        *immunology* 2016; 1.

568

**Figure Legends:**

570 **Fig.1. Study design.** (**A**) Blood samples from sepsis patients (S) (n=17) or non-infected post-cardiothoracic surgery patients (NIC) (n=12) were enrolled in the discovery cohort of the study, in addition, blood samples were obtained from healthy donors (HD) (n=11) and bone marrows biopsies from orthopedic surgery patients (BM) (n=5). Immunostainings targeting 42 parameters were performed and analyzed by mass cytometry. A computational "discovery strategy" was used to identify sepsis-specific subsets (**B**), a "computational validation" analysis was used to check whether the identified sepsis-specific subsets are strategy-dependant (**C**), and with an additional "expert driven validation" we defined a small set of markers to gate on the sepsis-specific neutrophil subsets (**D**). A second independent validation cohort, with sepsis patients (S) (n=24) and noninfected patients (NIP) (n=18), was used for the "biological validation" of these sepsis-specific neutrophil subsets by conventional flow cytometry (**E**).

581 **Fig.2. Identification of sepsis day 1-specific neutrophils with a discovery analysis strategy. (A)** t-SNE analysis was performed on neutrophils from all samples with cells being organized along t-SNE-1-2

583    and t-SNE-2-2 according to per-cell expression of CD11b, CD66b, CD16, CD10, CD64 and CD123,

584    PD-L1. Cell density for the concatenated file of each group is shown, on a black to yellow heat scale,

585    for each group time-point. (**B**) A heat map shows samples clustering (columns) according to nodes

586    cell proportion log2-transformed and centered around the mean proportion of all samples' nodes

587    (rows). Samples and mean-centered log2-transformed nodes cell proportion were arranged according

588    to complete linkage hierarchical clustering. Heat intensity (from blue to yellow) reflects the mean-

589    centered log2-transformed cell proportion of each sample's node. (**C**) A heatmap shows

590    characterization of cell nodes identified by SPADE (columns) according to mean expression of 7

591    markers (rows). Markers were arranged according to complete linkage hierarchical clustering and

592    nodes were pre-ordered according to (**B**) heat map nodes order. Heat intensity (from blue to red)

593    reflects the mean expression of each marker for each node. (**D**) Four groups of nodes were back-

594    viewed on t-SNE1-2 / t-SNE2-2 map. (**E**)  cells abundance of each meta-cluster subset (CD10-

595    CD64+CD16+PD-L1+ cell subset in red, CD10-CD64+CD16lowCD123+ cell subset in blue and

596    CD10-CD64+ cell subset in green) was presented as cell proportion among total neutrophils of each

597    group samples. Statistics: Nonparametric two-tailed Mann-Whitney test was used to compare

598    differences in cellular abundance of cell subsets between NIC-D1 and S-D1 (see the Methods

599    section). Sample sizes: HD=11, BM=5, NIC=12 and S=17.

600    **Fig.3. Validation of sepsis day-1-specific neutrophil subsets by a second computational strategy.** As

601    a first step, UMAP analysis was performed on all samples neutrophils and cells were organized along

602    UMAP-1 and UMAP-2 axes according to per-cell expression of CD11b, CD66b, CD16, CD10, CD64

603    and CD123, PD-L1. As a second step, FlowSOM clustering was done to separate neutrophils subsets

604    into 50 clusters. MEM was then used to quantify the enriched features of the 50 clusters. Protein

605    enrichment was reported on a +10 to −10 scale, where +10 indicates that protein's expression was

606      especially enriched and −10 indicated that the protein's expression was excluded from those cells,

607      relative to the other neutrophils clusters. (**A**) Among these clusters, two meta-clusters were identified

608      as phenotypically identical to the strategy-1 sepsis-specific neutrophils: clusters 18 and 19 (in red)

609      composed of CD10-CD64+PD-L1+ neutrophils and clusters 6 and 7 (in blue) composed of CD10-

610      CD64+ CD16lowCD123+ neutrophils. (**B**)   Cells abundance of each meta-cluster subset (CD10-

611      CD64+CD16+PD-L1+ cell subset in red and CD10-CD64+CD16lowCD123+ cell subset in blue) was

612      presented as cell proportion among total neutrophils of each group samples. Statistics: Nonparametric

613      two-tailed Mann-Whitney test was used to compare differences in cellular abundance of cell subsets

614      between NIC-D1 and S-D1 (see the Methods section). Sample sizes: HD=11, BM=5, NIC=12 and

615      S=17. (**C**) each meta-cluster cells (red and blue) was back-viewed on both UMAP-1 / UMAP-2 map,

616      and t-SNE1-2 / t-SNE2-2 map.

617 **Fig.4. Sepsis day 1-specific neutrophil subsets validated by expert gating correlate with severity**

618      **scores.** Expert gating strategy with 7 markers set (**A**) allowed the selection of CD10-CD64+PD-L1+

619      cell subset (in red) and CD10-CD64+CD16lowCD123+ cell subset (in blue), back-viewed on both

620      discovery (t-SNE1-2 / t-SNE2-2) and validation (UMAP-1 / UMAP-2) maps. The two neutrophil

621      subsets are significantly more abundant in sepsis patients (S) blood collected at day-1 post-admission

622      to ICU when compared to day-1 or day-7 non-infected post-cardiothoracic surgery patients (NIC) or

623      Healthy donors (HD) (**B**). Correlation between the log10 transformed frequency of $CD10^{-}CD64^{+}PD\text{-}$

624      $L1^{+}$ neutrophils subset (in red) or $CD10^{-}CD64^{+}CD16^{low}CD123^{+}$ neutrophils subset (in blue) and

625      SAPS II score (green squares) or SOFA score (purple squares) are shown in (**C**). ROC curve obtained

626      using only $CD123^{+}$ neutrophil subset is shown in (**D**) and the one using $CD123^{+}PD\text{-}L1^{+}$ neutrophil

627      subsets is shown in (**E**) and with the SOFA and SAPS II clinical scores are shown in (**F)** and (**G)**

628      respectively. Statistics: Nonparametric two-tailed Mann-Whitney test was used to compare cellular

629      abundances of cell subsets between S-D1 and NIC-D1, NIC-D7 or HD. Nonparametric two-tailed

630      Wilcoxon signed-rank test was used to compare cellular abundances between the two matched groups

631      S-D1 and S-D7. Linear regression lines and Spearman's rank correlation were used to assess

632      relationship between neutrophil subsets frequency and severity scores (see the Methods section).

633      Spearman r and tow-tailed $p$ value are presented. * $p<0.05$.  Sample sizes: HD=11, BM=5, NIC=12

634      and S=17.

635   **Fig.5. Non-neutrophil cells analysis resume sepsis immune hallmarks. (A)**  Lymphocytes and

636      monocytes numbers and intensity of HLA-DR expression on monocytes (mHLA-DR) were obtained

637      from non-neutrophils computational analysis and presented for each group. **(B)**  Neutrophils numbers

638      were obtained previously from the computational separation of neutrophils from non-neutrophil cells

639      and used to calculate Neutrophils/Lymphocytes ratio. Cell number of the main immune subsets that

640      were differentially abundant in S group from HD and NIC were presented in **(C)** and the ones that

641      were differentially abundant in S group from only HD were presented in **(D)**.

642   **Fig.6. Sepsis-specific neutrophils are detectable by conventional cytometry and discriminate**

643      **infected from non-infected patients.** The gating strategy applied on fluorescent flow cytometry data

644      of three sepsis patients from the validation cohort is showed in (**A**). The overlay of full minus-two

645      (FMT) stained control and the full panel (FP) stained tubes of each representative patient, showed the

646      increase of sepsis-specific neutrophil subsets with the decrease of CD10 expression by neutrophils

647      (CD14-CRTH2-CD15+ cells). The ROC curves were obtained using only CD123$^+$ neutrophil subset

648      (**B**), the two CD123$^+$ and PD-L1$^+$ neutrophil subsets **(C)** or using the SOFA **(D)** and SAPS II **(E)**

649      clinical scores.

650 **Fig.7. Staphylococcus aureus and Zymosan specific activation and phagocytosis are impaired in**

651      **immature sepsis neutrophils.** To address sepsis immature (CD64+CD10-) neutrophils phagocytic

652      capacities, 100µL of blood were incubated with 20µL or 40µL of beads coated with Staphylococcus

653      aureus or Zymosan, respectively, coated-particles and coupled with pH acidification-sensitive

654      fluorochrome. After 1h incubation at 37°C (PC: positive control) or 4°C (NC: negative control) cells

655      were stained and analyzed by flow cytometry. (**A**) represents gating strategy of CD15+CD14-CD3-

656      CD19- neutrophils from healthy donors (HD), sepsis day-1 samples (S-D1) and bone marrow samples

657      (BM). Cells were separated in 2 gates based on CD10 expression and phagocytosis marker intensity

658      (Staphylococcus aureus or Zymosan) and cells from PC (red dots) were overlaid on NC cells (blue

659      dots). The proportion of total phagocytic neutrophils were presented for the three groups.  t-SNE

660      analysis organized cells along t-SNE axes according to per-cell expression of 5 proteins and

661      phagocytosis fluorescence. Cell expression of CD11b after Staphylococcus aureus (**B**) or Zymosan

662      (**C**) stimulations, for one representative individual of HD and S-D1 stimulated at +4°C (NC) and

663      +37°C (PC) is shown on a heat scale. The ratio between PC and NC CD66b CD11b and particles

664      MFI, of each individual after Staphylococcus aureus (**D**) or Zymosan (**E**) stimulations, in each group

665      were plotted in histograms. CD10- cells have less phagocytic capacity whatever it is appreciated by

666      MFI or proportion. Stimulated CD10- cells exhibit a lower level of expression of CD11b and CD66b.

667      Statistics: Nonparametric two-tailed Mann-Whitney test was used to compare differences in cellular

668      abundance of cell subsets and MFI ratios (see the Methods section). Sample sizes: HD=4, S-D1=6
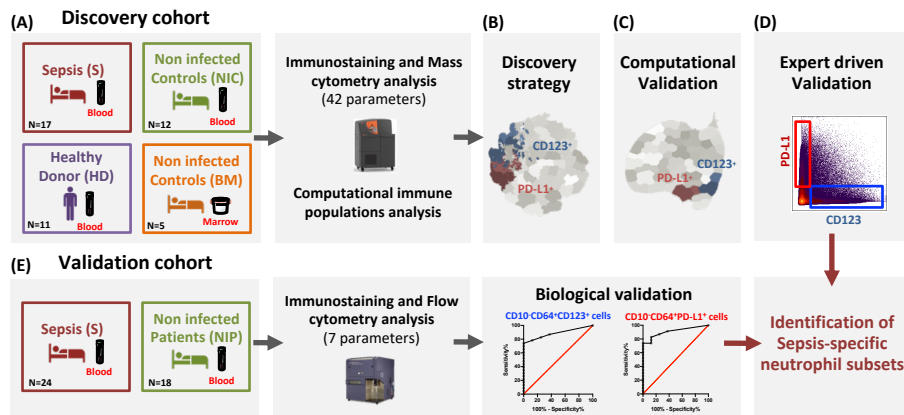
669      and BM=3.

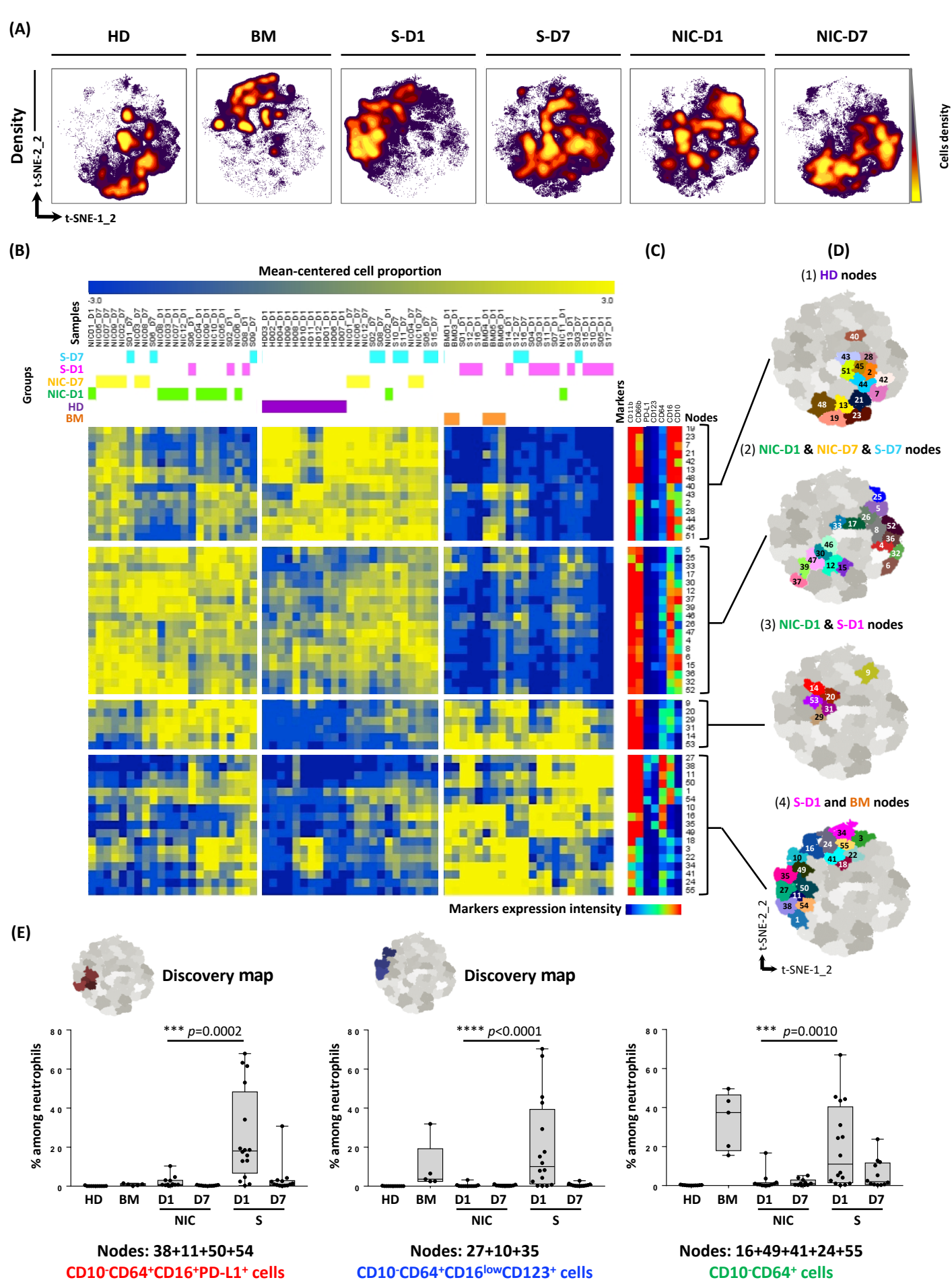670 **Figures:**

Figure 1. Study design

Figure 2. Identification of sepsis day 1-specific neutrophils with a discovery analysis strategy
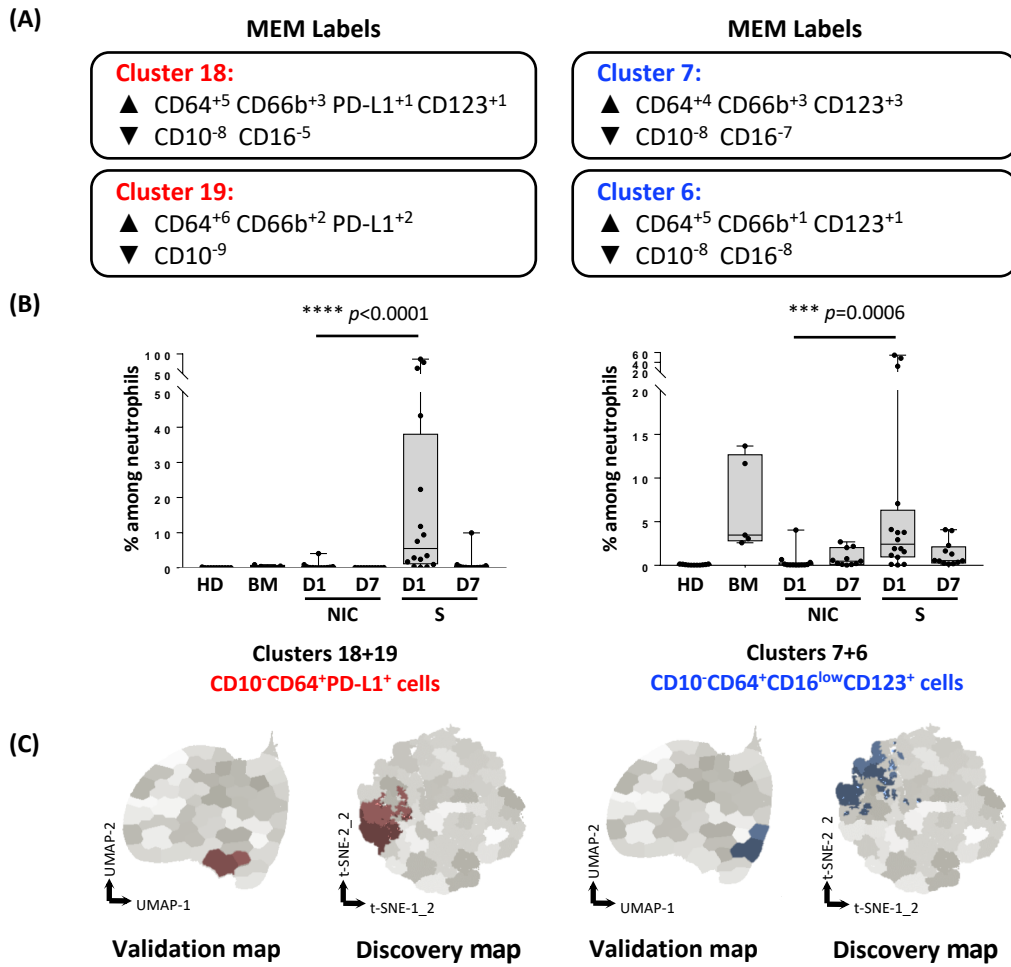
**(A)**

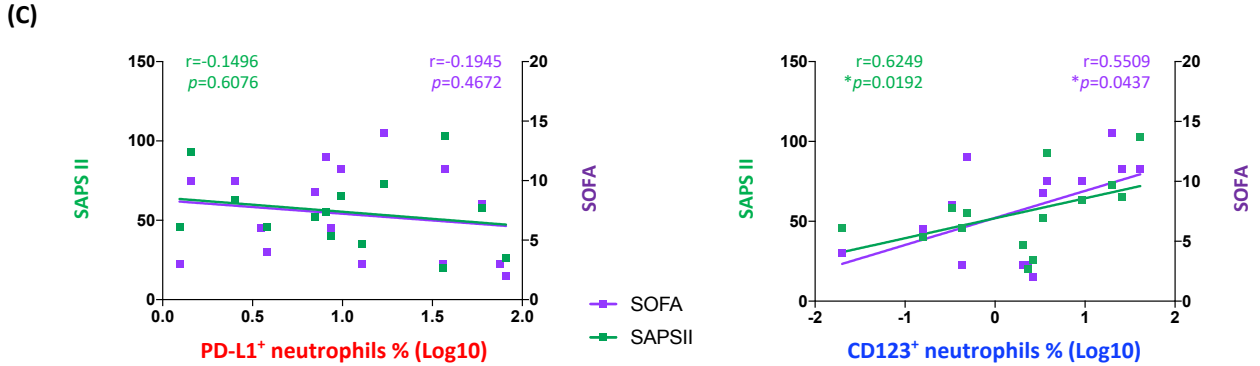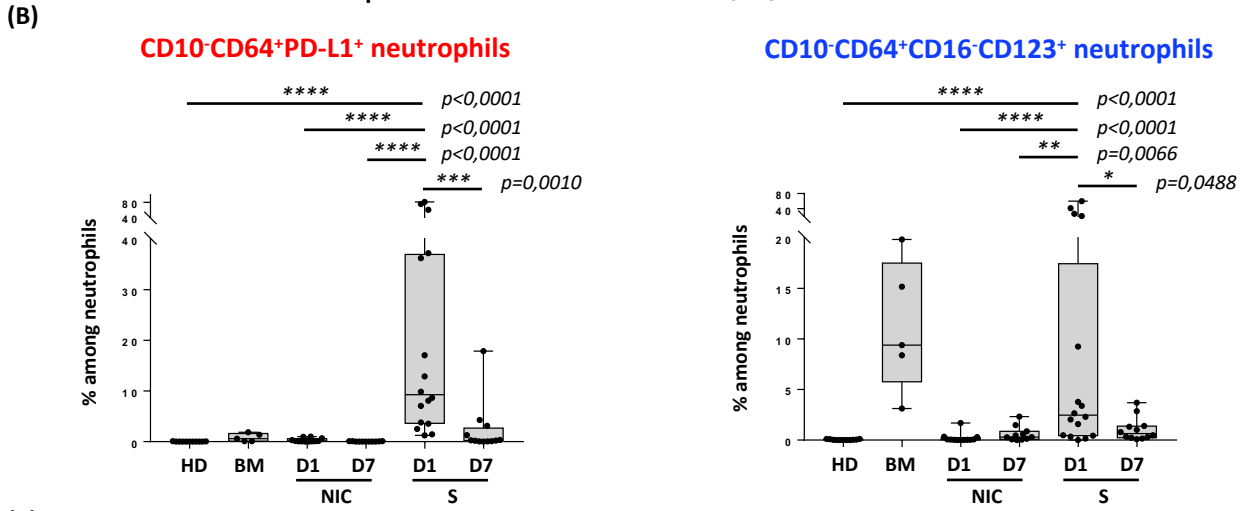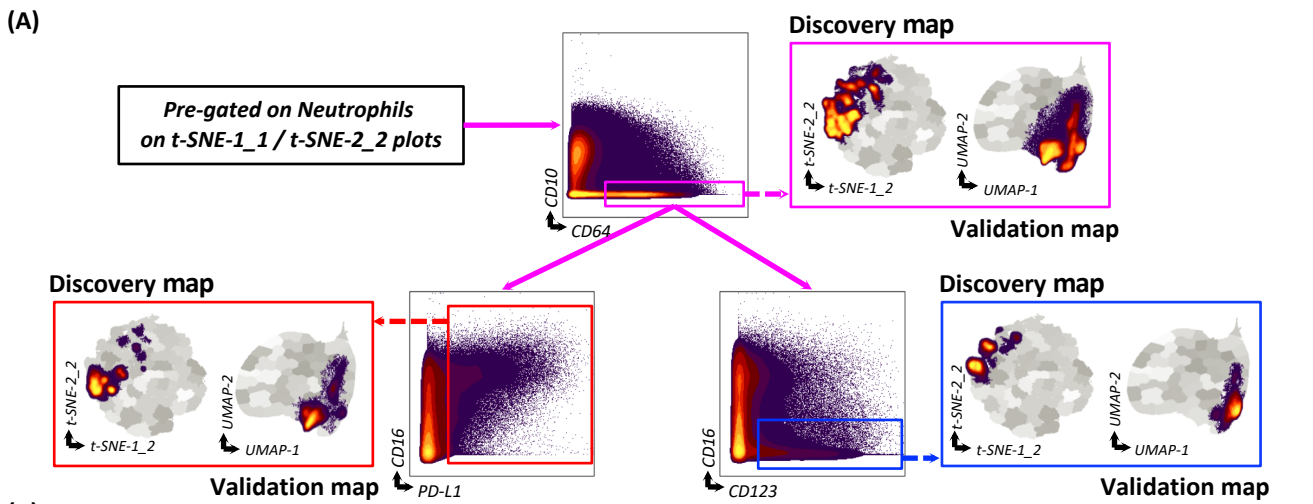| MEM Labels | MEM Labels |
|---|---|
| **Cluster 18:**<br>▲ CD64$^{+5}$ CD66b$^{+3}$ PD-L1$^{+1}$ CD123$^{+1}$<br>▼ CD10$^{-8}$ CD16$^{-5}$ | **Cluster 7:**<br>▲ CD64$^{+4}$ CD66b$^{+3}$ CD123$^{+3}$<br>▼ CD10$^{-8}$ CD16$^{-7}$ |
| **Cluster 19:**<br>▲ CD64$^{+6}$ CD66b$^{+2}$ PD-L1$^{+2}$<br>▼ CD10$^{-9}$ | **Cluster 6:**<br>▲ CD64$^{+5}$ CD66b$^{+1}$ CD123$^{+1}$<br>▼ CD10$^{-8}$ CD16$^{-8}$ |

**(B)**



Clusters 18+19
CD10$^{-}$CD64$^{+}$PD-L1$^{+}$ cells

Clusters 7+6
CD10$^{-}$CD64$^{+}$CD16$^{low}$CD123$^{+}$ cells

**(C)**



**Figure 3. Validation of sepsis day-1-specific neutrophil subsets by a second computational strategy**
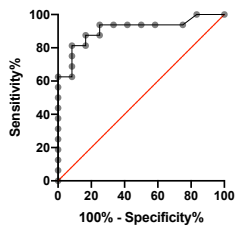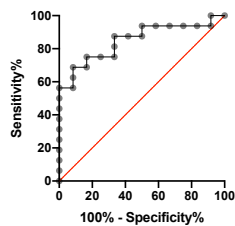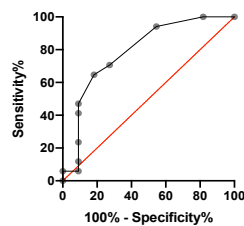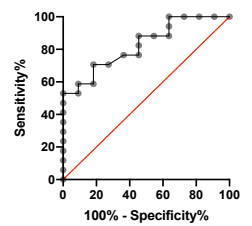
Figure 4. Validation of sepsis day 1-specific neutrophil subsets by expert gating

**(A)**

Lymphocytes number (*10^9/L)
*** p=0.0001
*** p=0.0003
* p=0.0315
HD | D1 D7 | D1 D7
NIC | S

Monocytes number (*10^9/L)
* p=0.0426
* p=0.0449
** p=0.0059
HD | D1 D7 | D1 D7
NIC | S

mHLA-DR intensity
**** p<0.0001
** p=0.0034
HD | D1 D7 | D1 D7
NIC | S

**(B)**

Neutrophils number (*10^9/L)
** p=0.0039
**** p<0.0001
*** p=0.001
HD | D1 D7 | D1 D7
NIC | S

Neutrophils/Lymphocytes ratio
** p=0.0039
**** p<0.0001
*** p=0.001
HD | D1 D7 | D1 D7
NIC | S

**(C)**

HLD-DR+CD14+ monocytes
**** p<0.0001
** p=0.0038
**** p<0.0001
HD | D1 NIC | D1 S

CCR2+CD25+CCR6+/low CD4+ T lymphocytes
**** p<0.0001
**** p<0.0001
* p=0.0380
HD | D1 NIC | D1 S

CCR2+CCR5int CCR6low/- CD8+ T lymphocytes
**** p<0.0001
**** p<0.0001
* p=0.0322
HD | D1 NIC | D1 S

HLD-DRlow CXCR5low CD19lowCCR6low B lymphocytes
* p=0.0317
*** p=0.0008
HD | D1 NIC | D1 S

mDC
** p=0.0033
* p=0.0130
HD | D1 NIC | D1 S

**(D)**

Basophils
**** p<0.0001
*** p=0.0003
HD | D1 NIC | D1 S

Eosinophils
**** p<0.0001
**** p<0.0001
HD | D1 NIC | D1 S

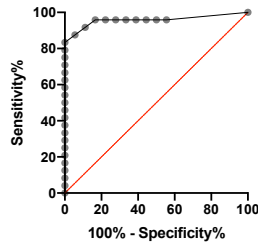**Figure 5. Non-neutrophil cells analysis resume sepsis immune hallmarks**
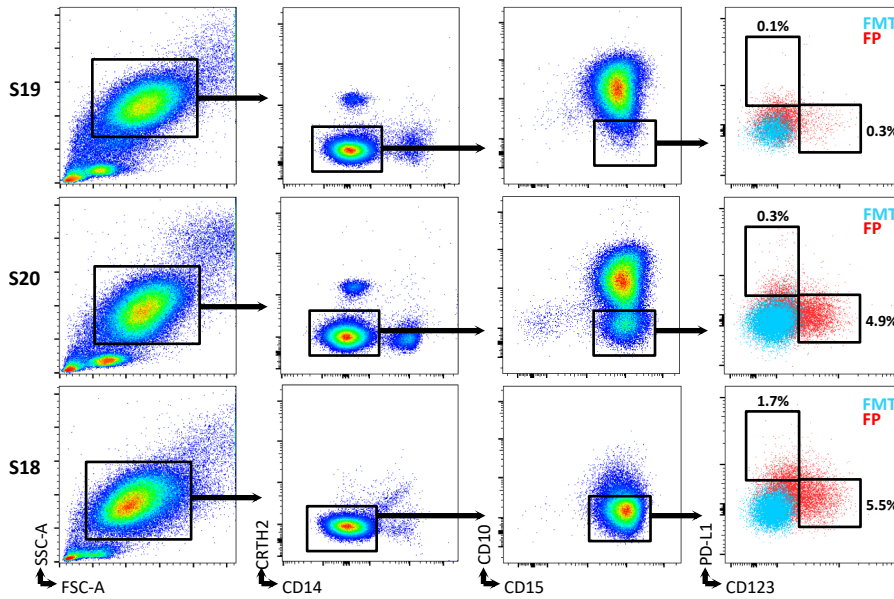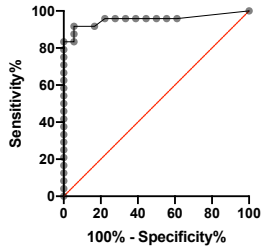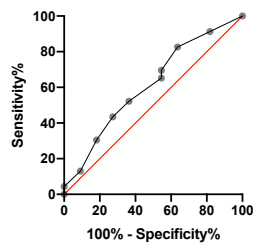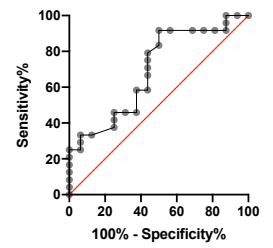
Figure 6. Sepsis-specific neutrophils are detectable by conventional cytometry and discriminate infected from non-infected patients
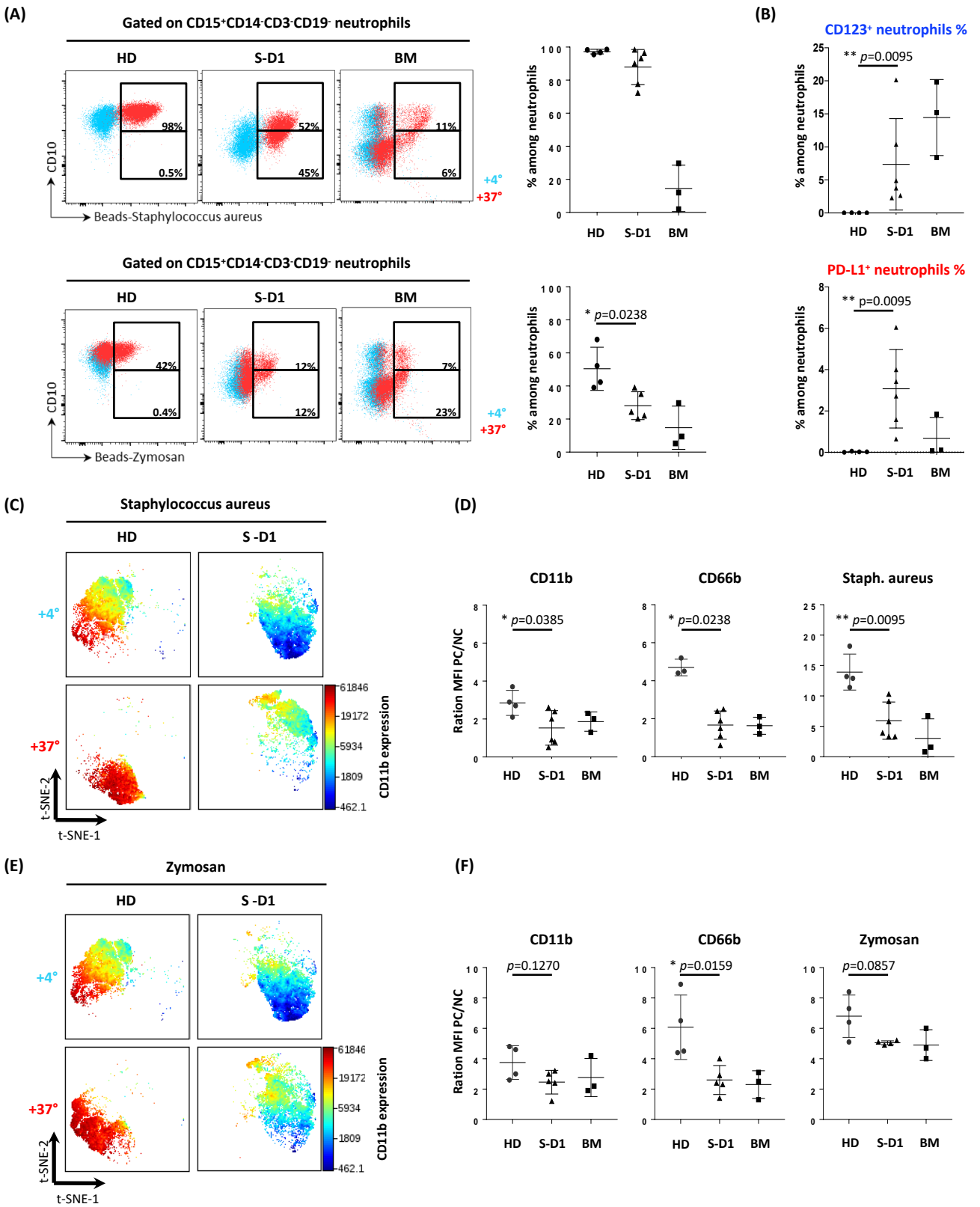
Figure 7. Staphylococcus aureus and Zymosan specific activation and phagocytosis are impaired in immature sepsis neutrophils